AUGUST 1978 PPPL-1447

UC-20f

TECHNIQUES FOR THE RECONSTRUCTION OF TWO-DIMENSIONAL IMAGES FROM PROJECTIONS

MASTER

BY

N. R. SAUTHOFF AND S. VON GOELER

PLASMA PHYSICS LABORATORY

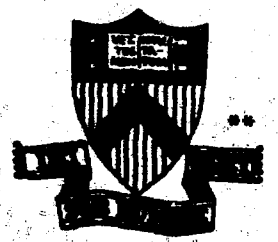

PRINCETON UNIVERSITY
PRINCETON, NEW JERSEY

This work was supported by the U. S. Department of Energy Contract No. EY-76-C-02-3073. Reproduction, translation, publication, use and disposal, in whole or in part, by or for the United States Government is permitted.

Techniques for the Reconstruction of Two-Dimensional Images from Projections

N. R. Sauthoff and S. von Goeler
Plasma Physics Laboratory, Princeton University
Princeton, New Jersey 08540

ABSTRACT

Several plasma diagnostics techniques measure the line integrals of quantities such as densities and optical, ultraviolet, and X-ray emission. Some approaches for reconstructing the local quantities from their line integrals, based on methods utilized in computerized tomography, electron microscopy, holographic interferometry, and radio astromomy, are derived and presented. Results for the special cases with source functions possessing helical symmetry - ranging from DNA to MHD - are emphasized.

I. Introduction

The derivation of local cylindrically-symmetric source functions from projected intensities, called Abel inversion [1,2], has been an essential part of many plasma physics methods, ranging from optical [3] to X-ray spectroscopy [4]. Recently, interest has been expressed in the analysis of sources which do not possess cylindrical symmetry, either because the equilibrium (as in PDX or Doublet) [5] or perturbations of the equilibrium (such as MHD modes) [6,7], violate the symmetry condition. In these cases, more general techniques are required for the reconstruction of two-dimensional images from projections.

Similar methods have been developed for other applications. In radio astronomy, Bracewell [8] developed a technique for producing a two-dimensional map of celestial sources of radio emission using an antenna with resolution in only one direction. In holographic interferometry, Sweeney, et al. [9,10] measured temperature distributions. In electron microscopy, De Rosier and Klug [9], De Rosier and Moore [10], and Lake [11] developed methods for reconstructing helically-symmetric biological structures such as ribonucleoprotein particles. The application which has given rise to the most extensive literature has been computerized tomography [12-14], wherein either the transmission of externally-produced radiation or the concentration of radioactive sources is measured in an effort to produce images of human organs by non-intrusive means. Various algorithms of general utility have also been discussed [15-21].

In a mathematical sense, the problem can be reduced to determining a function $f(r,\theta)$ given the projections $I(s,\phi)$, where s is the one-dimensional variable perpendicular to the line of sight and ϕ is the continuous variable describing the viewing angles, as shown in Figure 1. Radon [22-24] in 1917 first solved the equations governing such image reconstruction, demonstrating that if a complete set of projections $I(s,\phi)$ were available, the source function $f(r,\theta)$ could be uniquely determined. However, in a practical sense, a view of the object from every angle (ϕ) is not generally available, unless some assumption such as rigid rotation is invoked. In these situations, the technique for reconstruction must be chosen on the basis of applicability for a given class of source functions.

In this paper, several analytic techniques for the inversion of projections of helically-symmetric sources are described. Iterative methods, such as algebraic reconstruction [2], which are more suitable for sources localized more in real-space than in transform-space [25-26], will be omitted.

In Section III. A. the inversion technique for m=0, 1, 2, and 3, formerly used for the reconstruction of MHD tearing modes in the PLT tokamak [27] will be described; in Section III. B. a general technique due to Cormack [20,21] will be outlined; in Section III. C. a general Fourier transform technique will be applied to cases with helical symmetry, giving a result equivalent to that of Cormack.

II. Formulation of the Problem

Figure 1 shows the geometry: a distribution of sources $f(x,y)$ is viewed by a detector system fixed with respect to a rotated frame (x',y') where

$$x = x'\cos\phi - y'\sin\phi \text{ and } y = y'\cos\phi + x'\sin\phi \ . \tag{1}$$

The detectors view along the y'-axis such chat the projected intensity along line x' with the coordinate system rotated at angle ϕ is

$$I(x',\phi) = \int_{-\infty}^{\infty} dy' \ f(x'\cos\phi - y'\sin\phi,\ y'\cos\phi + x'\sin\phi) \ . \tag{2}$$

The topic of later sections will be the inversion of this integral equation, given the set of projections $I(x',\phi)$.

The determination of the proper interpolation of $I(x',\phi)$ between observation points requires introduction of knowledge of the expected source functions. Sources which are localized spatially (such as tumors in the brain) result in a large number of components in an expansion in a set of "poloidal" harmonics:

$$I(x',\phi) = \sum_{m=0}^{\infty} I_m(x') \cos\left\{m\left[\phi - \phi_m(x')\right]\right\} \ ; \tag{3}$$

on the other hand, sources localized in k-space (such as MHD modes in tokamaks, or cross sections with only low multipole moments) by definition require only a small number of terms

in the expansion if the center of the rotating detector system coincides with the symmetry point of the source function (otherwise, multipole moments of the source are generated).

In general, the determination of the functions $I_m(x')$ and $\phi_m(x')$ can be made by Fourier analysis in the angular coordinate ϕ if the entire domain in ϕ is accessible. An equivalent separation can be achieved if the source is assumed to be rigidly rotating since the Doppler-shift gives a temporal frequency proportional to the spatial wavenumber-m. In more restricted cases, in which the intensity can be approximated by a finite number of harmonics, measurements at a finite number of angles can separate the harmonics; for example, if only an even and an odd source function are assumed to be present, the even and odd components of the intensities are the corresponding harmonics; similarly, some views at two angles are sufficient for two even or two odd modes, subject to aliasing criteria.

In the following sections, the functions $I_m(x')$ and $\phi_m(x')$ will be assumed to have been determined and the problem to have been reduced to the inversion of equation (2), given equation (3).

III. Reconstruction Techniques

III. A. Method for m=0, 1, 2, and 3 (Used in References [6] and [27]

Standard Abel-inversion techniques [1,2] utilize a coordinate system (as shown in Figure 2) wherein the intensity along

a chord tangent to a circle of radius r is calculated as a line integral of the emissivity at radius r_0 with path length given by:

$$ds = r_0 dr_0 / \sqrt{r_0^2 - r^2} \quad . \tag{4}$$

Extending the technique to situations where

$$f(r,\theta) = \sum_m f_m(r) \cos\left\{m\left[\theta - \theta_m(r)\right]\right\} \quad , \tag{5}$$

the expression for the intensity along a chord tangent at radius r and angle ϕ can be shown to be

$$I(r,\phi) = 2 \int_{r_0=r}^{\infty} \frac{r_0 dr_0}{\sqrt{r_0^2 - r^2}} \sum_m f_m(r_0) \cos\left\{m\left[\theta(r_0) - \theta_m(r_0)\right]\right\} \quad , \tag{6}$$

where

$$\theta(r_0) = \phi - \cos^{-1}(r/r_0) \quad . \tag{7}$$

Defining the functions

$$\begin{Bmatrix} f_{m,c}(r_0) \\ f_{m,s}(r_0) \end{Bmatrix} = f_m(r_0) \begin{Bmatrix} \cos\left[m\theta_m(r_0)\right] \\ \sin\left[m\theta_m(r_0)\right] \end{Bmatrix} \quad , \tag{8}$$

and

and

$$\begin{Bmatrix} I_{m,c}(r) \\ I_{m,s}(r) \end{Bmatrix} = I_m(r) \begin{Bmatrix} \cos(m\phi) \\ \sin(m\phi) \end{Bmatrix} , \tag{9}$$

it can be shown [7] that

$$\begin{Bmatrix} I_{m,c}(r) \\ I_{m,s}(r) \end{Bmatrix} = 2 \int_{r_0=r}^{\infty} \frac{r_0 dr_0 \; T_m(r/r_0)}{\sqrt{r_0^2 - r^2}} \begin{Bmatrix} f_{m,c}(r_0) \\ f_{m,s}(r_0) \end{Bmatrix} , \tag{10}$$

where $T_m(x)$ is the Chebyshev polynomial of order m [28]. The problem thus reduces to an inversion of the general equation

$$\psi(r) = 2 \int_{r_0=r}^{\infty} \frac{r_0 dr_0 \; T_m(r/r_0)}{\sqrt{r_0^2 - r^2}} \chi(r_0) , \tag{11}$$

which is a Volterra equation of the first kind [29]. Standard Abel inversion techniques suggest operating on both sides of the equation with

$$\int_u^{\infty} \frac{dr \; r \; P_m(r/u)}{r^2 - u^2} , \tag{12}$$

where $P_m(x)$ is a polynomial in x such that reversing the order of integration in the right hand side, the integration over the variable r reduces to a single power of u, which can in turn be removed from the integrand, permitting a simple differentiation of the limits on the right hand side.

With the particular choices,

$$P_0(x) = 1,\ P_1(x) = 1/x,\ P_2(x) = 1,\ P_3(x) = (1/x)(1 - 4/3\ x^2) \qquad (13)$$

the right hand sides can be integrated to yield

$$\int_u^\infty \frac{dr\ r\ P_m(r/u)}{\sqrt{r^2 - u^2}}\ \psi(r) = 2\int_u^\infty \frac{dr\ r\ P_m(r/u)}{\sqrt{r^2 - u^2}} \int_{r_0=r}^\infty \frac{dr_0\ r_0\ T_m(r/r_0)}{\sqrt{r_0 - r^2}}\ \chi(r_0)$$

$$= 2\int_u^\infty dr_0\ r_0\ \chi(r_0) \int_u^{r_0} \frac{dr\ r\ P_m(r/u)\ T_m(r/r_0)}{\sqrt{(r^2 - u^2)(r_0^2 - r^2)}}$$

$$= 2\int_u^\infty dr_0\ r_0\ \chi(r_0) \begin{cases} \dfrac{\pi}{2} & m=0 \\ \dfrac{u}{r_0}\ \dfrac{\pi}{2} & m=1 \\ +\dfrac{u^2}{r_0^2}\ \dfrac{\pi}{2} & m=2 \\ -\dfrac{u}{r_0}\ \dfrac{\pi}{6} & m=3\ . \end{cases} \qquad (14)$$

Moving to the left-hand side all u-dependence, with the exception of the integration limit, both sides can be differentiated to yield for each m:

$$\chi_0(u) = -\frac{1}{\pi}\ \frac{1}{u}\ \frac{d}{du} \int_{r=u}^\infty \frac{dr\ r\ \psi_0(r)}{\sqrt{r^2 - u^2}} \qquad (15)$$

$$\chi_1(u) = -\frac{1}{\pi}\frac{d}{du}\int_{r=u}^{\infty}\frac{dr\ \psi_1(r)}{\sqrt{r^2 - u^2}} \tag{16}$$

$$\chi_2(u) = -\frac{1}{\pi}u\frac{d}{du}\frac{1}{u^2}\int_{u}^{\infty}\frac{dr\ r\ \psi_2(r)}{\sqrt{r^2 - u^2}} \tag{17}$$

$$\chi_3(u) = \frac{3}{\pi}\frac{d}{du}\int_{r=u}^{\infty}\frac{dr(1 - 4/3\ r^2/u^2)\ \psi_3(r)}{\sqrt{r^2 - u^2}} \quad . \tag{18}$$

The singularities at r=u in each expression for odd-m are, in fact, integrable since $\psi(r) \sim r$. This technique of differentiating an integral of the raw data affords somewhat more noise immunity than those which differentiate prior to integration; in this sense, it is an extension of the work of Barr [2].

The digital implementation of this small-m method is described in Appendix I. Figure 3 shows the results of picking a source function, integrating to obtain the expected line integral, and using the inversion formulae to estimate the original source function. For m=0,1,2, the result is satisfactory; for m=3 a divergence near the origin is encountered due to the approximation of the line integral in the inversion.

III. B. Series Expansion Method

A technique closely related to that in Section III. A. is that of Cormack [20,21] in which the function $I(x',\phi)$ is again divided into two components for each m. The difference lies in

the introduction of a pole in the integrand at the origin during the inversion. Instead of utilizing the operator in equation (12), the Cormack method uses on equation (11) the operator

$$\int_{r=u}^{\infty} \frac{dr\ T_m(r/u)}{\sqrt{r^2 - u^2}} u/r \tag{19}$$

to yield (after changing the order of integration):

$$\int_{r=u}^{\infty} \frac{dr\ T_m(r/u)}{\sqrt{r^2 - u^2}} u/r\ \psi(r) = 2 \int_{r_0=u}^{\infty} dr_0\ \chi(r_0) \int_{r=u}^{r_0} \frac{dr\ T_m(r/u)\ T_m(r/r_0)}{\sqrt{(r_0^2 - r^2)(r^2 - u^2)}} \frac{ur_0}{r} \tag{20}$$

As stated in the reference, using recurrence relations and expressions for $T'_m(x)$ and $T''_m(x)$ in terms of $T_{m-1}(x)$ and $T_m(x)$, the second integral on the right hand side can be shown to equal $\pi/2$; therefore

$$\chi(u) = -\frac{1}{\pi} \frac{d}{du} \int_{r=u}^{\infty} \frac{dr\ T_m(r/u)\ u/r\ \psi(r)}{\sqrt{r^2 - u^2}} \quad . \tag{21}$$

For m=1, the expression for $\chi(u)$ agrees with that of the previous section.

This expression for general-m can also be derived by Hankel transforms as described by Cormack [21].

The digital implementation of equation (21) is somewhat more difficult; if, as described in Appendix II, FINT(r) is expanded as $(A_j + B_j r^2)$ in each radial interval, and $T_m(r/u)$ is expanded in powers of (r/u), then the integral FUNC(r) can be analytically performed using a routine to evaluate $\int dx\ \sec^{2n}(\theta)$.

However, terms of the form $1/u^L$, $L > 0$, appear and cause divergences at the origin. This divergence can be traced to the approximation used for FINT(r). Examples are shown in Figure 4.

A convergent expansion for FUNC(r) can be obtained by expanding FINT(r) as

$$\text{FINT}(r) = \alpha \frac{T_m(\beta r)}{\sqrt{1 - \beta^2 r^2}} ; \tag{22}$$

however, the fitting of the function to this form is at best difficult, and for some m impossible (consider nodes for small m).

Another approach for integrating equation (21) has been suggested by Cormack [21], who expanded the line integral data as

$$\psi(r) = 2a \sum_{\ell=0}^{\infty} a_m^{\ell} \sin\left[(m + 2\ell + 1) \cos^{-1}(r/a)\right] \tag{23}$$

and determined the local function to be

$$\chi(r_0) = \sum_{\ell=0}^{\infty} (m + 2\ell + 1)\, a_m^{\ell}\, R_m^{\ell}(r_0/a) \tag{24}$$

where $R_m^{\ell}(x)$ is the Zernicke polynomial [30]

$$R_m^{\ell}(x) = \sum_{s=0}^{\ell} \frac{(-1)^s (m + 2\ell - s)!\, x^{m + 2\ell - 2s}}{s!\,(m + \ell - s)!\,(\ell - s)!} . \tag{25}$$

This method has the advantages of (1) forcing the approximated line integral to possess the correct number of nodes, and (2) minimizing errors by the least squares fitting implicit in orthogonal expansions.

Figure 5 shows examples of this technique for various values of m. The applicability of this method to large m's is apparent. The details of the fit are discussed in Appendix III.

Figure 6 shows the same source functions as in Figure 5, except the line integral array has been multiplied by a function differing from unity by a random amount of maximum amplitude 25%. This illustrates the noise immunity for this method. For fewer data points the sensitivity to error is increased.

III. C. Fourier Transform Technique

The two previous methods involved an expansion of the source and projection into "poloidal" harmonics; in contrast, a third technique based on the Fourier transform gives an expression for the local source function which consists of a double integral over k-space of the one-dimensional Fourier transform of the projection at a related angle.

The fundamental observation is that the one-dimensional Fourier transform of the projection at rotation angle ϕ is proportional to the two-dimensional transform of the source function at angle ϕ in k-space. As shown in Figure 1, the projection along the y'-axis at distance x' along the perpendicular to the line of sight is given by equation (2). Defining the transform pair as

$$F(k) = \int_{-\infty}^{\infty} dx \; e^{-ikx} f(x), \; f(x) = \frac{1}{2\pi} \int_{-\infty}^{\infty} dk \; e^{ikx} F(k) \quad , \qquad (26)$$

the transform of $I(x',\phi)$ is

$$\int_{-\infty}^{\infty} dx' e^{-ikx'} I(x',\phi) = \int_{-\infty}^{\infty} dx' \int_{-\infty}^{\infty} dy' e^{-ikx'} f(x,y) . \tag{27}$$

Transforming to the coordinate system (x,y) in the right-hand side, the Jacobian being unity,

$$\begin{aligned} \int_{-\infty}^{\infty} dx' e^{-ikx'} I(x',\phi) &= \int_{-\infty}^{\infty} dx \int_{-\infty}^{\infty} dy\, e^{-ik[x\cos\phi + y\sin\phi]} f(x,y) \\ &= F(k\cos\phi, k\sin\phi) . \end{aligned} \tag{28}$$

Hence, the Fourier transform of the source function at wavevector of magnitude k and angle ϕ is equal to the transform of the projection at rotation angle ϕ. Using the transform pair in equation (26), an expression for the source function at radius r and spatial angle ϕ can be shown to be

$$f(r,\theta) = \frac{1}{(2\pi)^2} \int_0^{\infty} dk\, k \int_0^{2\pi} d\phi\, e^{ikr\cos(\phi-\theta)} \int_{-\infty}^{\infty} dx'\, e^{-ikx'} I(x',\phi) . \tag{29}$$

In general, fast Fourier transforms can be used to determine the source function given the projections.

The special case of helical symmetry with cross section perpendicular to the axis of the helix, as expressed in equation (3) with a single-m, is

$$f_m(r,\theta) = \frac{1}{8\pi^2} \int_0^\infty dk\ k \int_{-\infty}^{\infty} dx' I_m(x') e^{-ikx'} \int_0^{2\pi} d\phi\ e^{ikr\cos(\phi-\theta)} \left\{ e^{im[\phi-\phi_m(x')]} + e^{-im[\phi-\phi_m(x')]} \right\} \tag{30}$$

By the expansion of the first exponential in the right integral by the Bessel function identity [31] familiar to plasma physicists from the expansion of the orbit integral of a particle in groharmonics,

$$f_m(r,\theta) = \frac{i^m}{2\pi} \int_0^\infty dk\ k \int_{-\infty}^{\infty} ds\ I_m(s)\ e^{-iks} J_m(kr) \cos\left\{ m[\theta-\phi_m(s)] \right\}. \tag{31}$$

Converting to an integral over positive-s,

$$f_m(r,\theta) = \frac{(-i)^m}{\pi} \int_0^\infty ds\ I_m(s) \cos\left\{ m[\theta-\phi_m(s)] \right\} \int_0^\infty dk\ k\ J_m(kr) \begin{cases} \cos(ks) & m=\text{even} \\ i\sin(ks) & m=\text{odd}. \end{cases} \tag{32}$$

Using the separation into orthogonal components as in equations (8) and (9), this reduces to the equation

$$\chi(r) = \frac{(-i)^m}{\pi} \int_0^\infty ds\ \psi(s) \int_0^\infty dk\ k\ J_m(kr) \begin{cases} \cos(ks) & m=\text{even} \\ i\sin(ks) & m=\text{odd}. \end{cases} \tag{33}$$

Eliminating the k in the second integral by substituting derivations of trigonometric functions and integrating by parts, we obtain

$$\chi(r) = \frac{-(-i)^m}{\pi} \int_0^\infty ds\ \psi'(s) \int_0^\infty dk\ J_m(kr) \begin{cases} \sin(ks) & m=\text{even} \\ -i\cos(ks) & m=\text{odd}. \end{cases} \tag{34}$$

Using tables of integrals of Bessel functions or Hankel transforms, expressions for the right-hand integral can be found; expressing them in terms of Chebyshev polynomials of the first and second kinds, manipulating them as done by Cormack in showing that the Hankel transform of his equation (10) gives his equations (6) a[illegible] [21], equation (32) can be shown to be equivalent to equations (10) and (21).

Hence the general Fourier transform technique from computed tomography [18, 32] reduces to the Cormack approach in those cases where the line integrals possess the symmetry given by equation (3).

This last technique, given by equations (23)-(25), appears to be the most preferable method for the cases of moderate-m source functions.

IV. Conclusion

Two forms for the inversion of the line intergrals encountered in reconstructing source functions with symmetry $\cos(m\theta)$ have been derived and examples of results with trial functions given.

The first form, equations (15)-(18), is applicable to cases with m=0,1,2, or 3. The numerical implementation consists of integration over raw data points and a smoothing derivative; acceptable results are obtained for m=0, 1, and 2; a singularity at the origin restricts use for m=3.

The second form, equation (21), has been derived by two techniques. Two numerical methods for its utilization have been presented; the first involves a numerical integration of the raw data followed by a derivative and posesses the same difficulties as the first form solution; the second involves the expansion of the line integrals in a set of appropriate basis functions and the reconstruction of the local emissivity from the expansion coefficients.

Acknowledgments

The authors would like to thank W. Stodiek for his interest and support.

This work was supported under U.S. Department of Energy Contract EY-76-C-02-3073.

References

[1] K. Bockasten, J. Opt. Soc. Am. 51, 943 (1961).

[2] W. L. Barr, J. Opt. Soc. Am. 52, 885 (1962).

[3] W. J. Pearce in P. Dickerman [ed], Optical Spectroscopic Measurements of High Temperatures (Chicago: University of Chicago Press, 1960), p. 125.

[4] S. von Goeler, et al., Princeton University Plasma Physics Laboratory Report PPPL-1383 (1977).

[5] D. Meade and J. Sinnis, "The PDX Esperiment," Proceedings of the International Symposium on Plasma Wall Interactions (London: Pergamon Press, 1976).

[6] S. von Goeler, Proc. 7th European Conference on Plasma Physics and Controlled Nuclear Fusion (Lausanne, 1975) II 71.

[7] N. R. Sauthoff, Proceedings of the Society of Photo-Optical Instrumentation Engineers 106, 40 (1977).

[8] D. W. Sweeney and C. M. Vest, Appl. Opt. 11, 205 (1972); Appl. Opt. 12, 2649 (1973).

[9] D. J. DeRosier and A. Klug, Nature 217, 130 (1968).

[10] D. J. DeRosier and P. B. Moore, J. Mol. Biol. 52, 355 (1970).

[11] J. A. Lake, J. Mol. Biol. 66, 255 (1972).

[12] Z. H. Cho [ed], IEEE Transactions on Nuclear Science NS-21, No. 3, Special Issue on "3-D Image Reconstruction" (1974).

[13] W. Swindell and H. H. Barrett, Physics Today 30, 32 (1977).

[14] R. A. Brooks and G. Di Chiro, Radiology 117, 561 (1975).

[15] R. Gordon and G. T. Herman, Int. Rev. Cytol. 38, 111 (1974).

[16] Z. H. Cho, I. Ahn, C. Bohm, and G. Huth, Phys. Med. Biol. 19, 511 (1974).

[17] G. T. Herman and S. W. Rowland, Computer Graphics and Image Processing 2, 151 (1973).

[18] Z. H. Cho, et al., IEEE Transcations on Nuclear Science NS-22, 344 (1975).

[19] M. V. Berry and D. F. Gibbs, Proc. Roy. Soc. Lond. A.314, 143 (1970).

[20] A. M. Cormack, J. Appl. Physics 34, 2722 (1963).

[21] A. M. Cormack, J. Appl. Physics 35, 2908 (1964).

[22] J. Radon, Berichte Der Gesellschaft Der Wissenschaften Zu Leipzig 69, 262 (1917).

[23] F. John, Plane Waves and Spherical Means Applied to Partial Differential Equations (New York; Interscience Publishers, Inc., 1955), 7.

[24] A. M. Cormack, Phys. Med. Biol. 18, 195 (1973).

[25] R. Gordon and G. T. Herman, op. cit., p. 142.

[26] Z. H. Cho, et al., op. cit., p. 346.

[27] N. R. Sauthoff, S. von Goeler, and W. Stodiek, Princeton University Plasma Physics Laboratory Report PPPL-1379 (1978); Nuclear Fusion (to be published).

[28] M. Abramowitz and I. A. Stegun, Handbook of Mathematical Functions, (Washington, D.C.: U.S. Government Printing Office, 1970) equation 22.3.15.

[29] P. M. Morse and H. Feshbach, Methods of Theoretical Physics (New York: McGraw-Hill Book Company, 1953), 905.

[30] M. Born and E. Wolf, Principles of Optics (London: Pergamon Press, 1959).

[31] M. Abramowitz and I. A. Stegun, op. cit., equations 9.1.42 and 9.1.43.

[32] A. M. Cormack (private communication).

[33] L. A. Shepp and B. F. Logan, IEEE Transactions on Nuclear Science NS-21, 21 (1974).

Appendix I

Program for Small - m Inversion Technique

The digital implementation of equations (15)-(18) involves the following steps.

(A) Form a regular array FINT(r) = (1,1,1/r) PSI(r) for m=(0,even,odd), where PSI(r) is the line integral array.

(B) Calculate the line integral FUNC(r) by sweeping over the radii, approximating FINT(r) by a polynomial $(A_j + B_j r^2)$ in each region $r_{j-1} < r < r_j$, and summing over the analytical integral for each region.

(C) If m=2, correct if FUNC(0) $\neq 0$. The shape used for this application was

$$\text{CORRECTION}(r) = -\text{FUNC}(0)\left[1-2\left(r/a\right)^2 + \left(r/a\right)^4\right], \tag{34}$$

which gave a correction on the local emission

$$\text{CHI}(r) \sim \frac{\text{FUNC}(0)}{\pi}\ \frac{1}{r^2}\ \left[1-\left(r/a\right)^2\right]. \tag{35}$$

(D) Differentiate the function FUNC(r) to obtain a function CHIREG(r) which is finite and even about the origin, using a routine

$$\text{CHIREG}(r) = \frac{1}{r^{NA}}\ \frac{d}{dr}\ \frac{1}{r^{NF}}\ \text{FUNC}(r) \tag{36}$$

where FUNC(r) has been approximated

$$\text{FUNC}(r) = \sum_{I=1}^{NT} C_I\ r^{N0+(I-1)ND} \tag{37}$$

over NP points near radius r_j given by $r_{j-NLEFT}$, $r_{j-NLEFT+1}$, ..., and NA=1, NT=3, ND=2, NP=5, NLEFT=2; for m $\neq$ 2, N0=0, NF=0; for m=2, N0=2, NF=2.

(E) Return to local function CHI(r)= $-(1/\pi)$ CHIREG(r) $(1,r^2,r)$ for m=(0,even,odd).

Appendix II

Application of Cormack Solution with Numerical Integration

The approach for the use of equation (21) taken in this section is similar to that in Appendix I.

(A) The array FINT(r) is formed.

(B) The array FUNC(r) is found by approximating FINT(r) by a polynomial $(A_j + B_j r^2)$ in each region and performing the sum of the analytic results in each region; this involves a routine to compute the integral of $\sec(\theta)^{2N}$.

(C) The array FUNC(r) is differentiated as in step (D) of Appendix I with NT=3, NF=0, NP=5, NLEFT=2; for m=0, ND=1, N0=0, and NA=0; for m=even, ND=3, N0=0, NA=2; for m=odd, ND=2, N0=0, NA=1.

(D) The local function CHI(r) is determined.

Appendix III

Expansion of Line Integral in Orthogonal Functions

The last Cormack method, given by equations (23) and (24), is easily programmed. The expansion in the basis set of sinusoidal functions can be done by a least squares approach and a matrix inversion for a small number of terms and by using orthogonality relations for large numbers of points and terms in the expansion.

FIGURE CAPTIONS

Figure 1. Coordinate systems and geometry. The source function $f(x,y)$ is viewed by a set of detectors viewing along the y' axis, resulting in the line integral function $I(x',\phi)$.

Figure 2. Geometry for the view of a source function $f(r_o,\theta)$ along a chord tangent at radius r. The output is a line integral along the line s.

Figure 3. Results of picking a source function (solid line), calculating the line integral (crossed line), and inverting the line integral by the small-m technique to give the estimated local source function (dotted line). Symmetries are (a) m=0, (b) m=1, and (c) m=2.

Figure 4. Results of inversion using Cormack formula with numerical integration and smoothing derivative. Symmetries are (a) m=0, (b) m=1, (c) m=2, and (d) m=3.

Figure 5. Results of inversion using Cormack formula with orthogonal expansion of line integral data. Symmetries are (a) m=0, (b) m=1, (c) m=2, (d) m=4, (e) m=8, and (f) m=12. Number of data points is 20.

Figure 6. Same as Figure 5, except line integral array has been multiplied by a random function differing from unity by a maximum of 25%. Number of data points is 15.

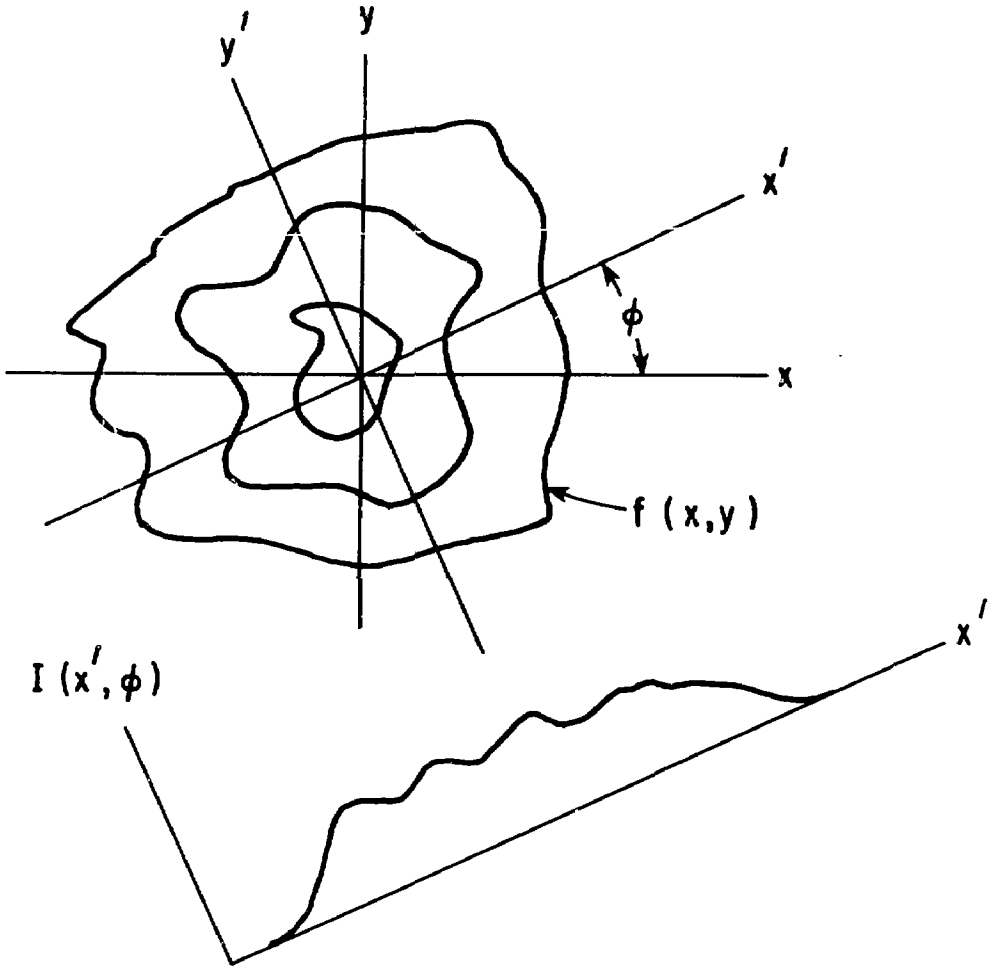

Fig. 1. 783651

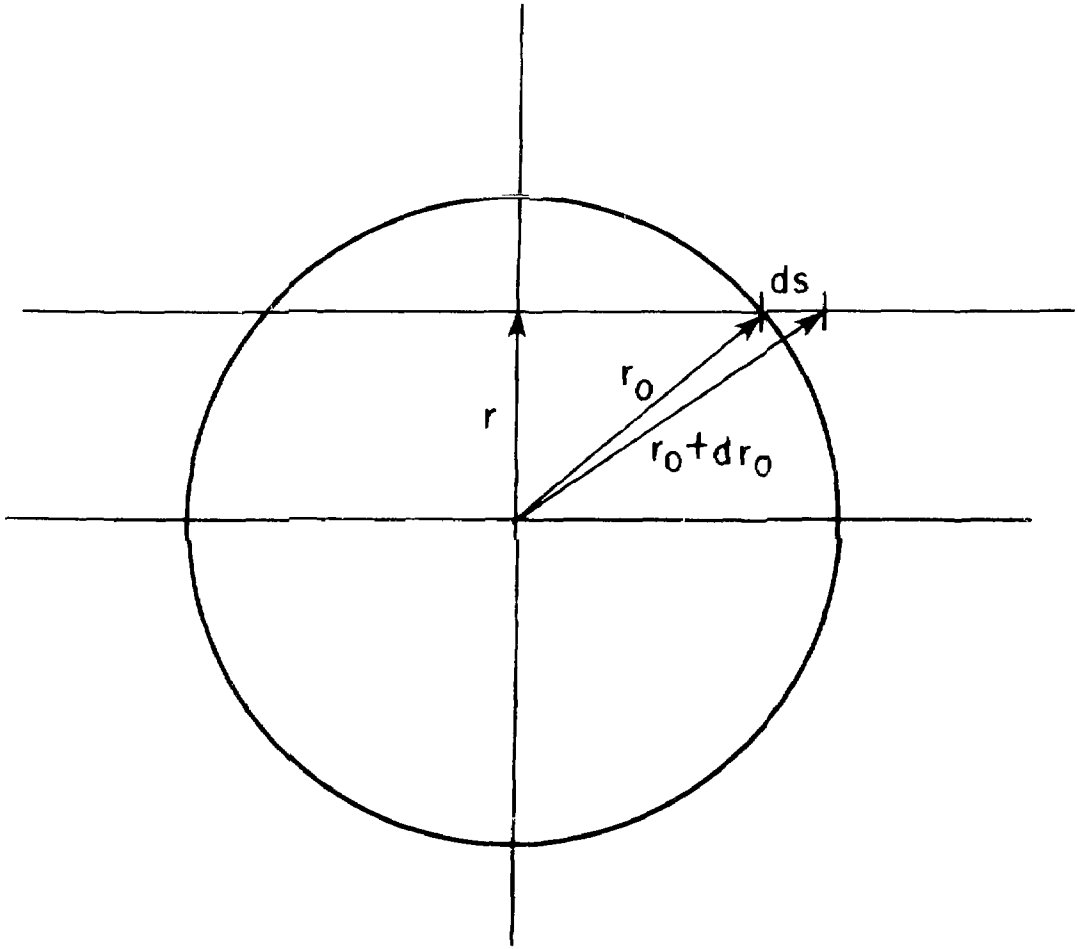

Fig. 2. 783650

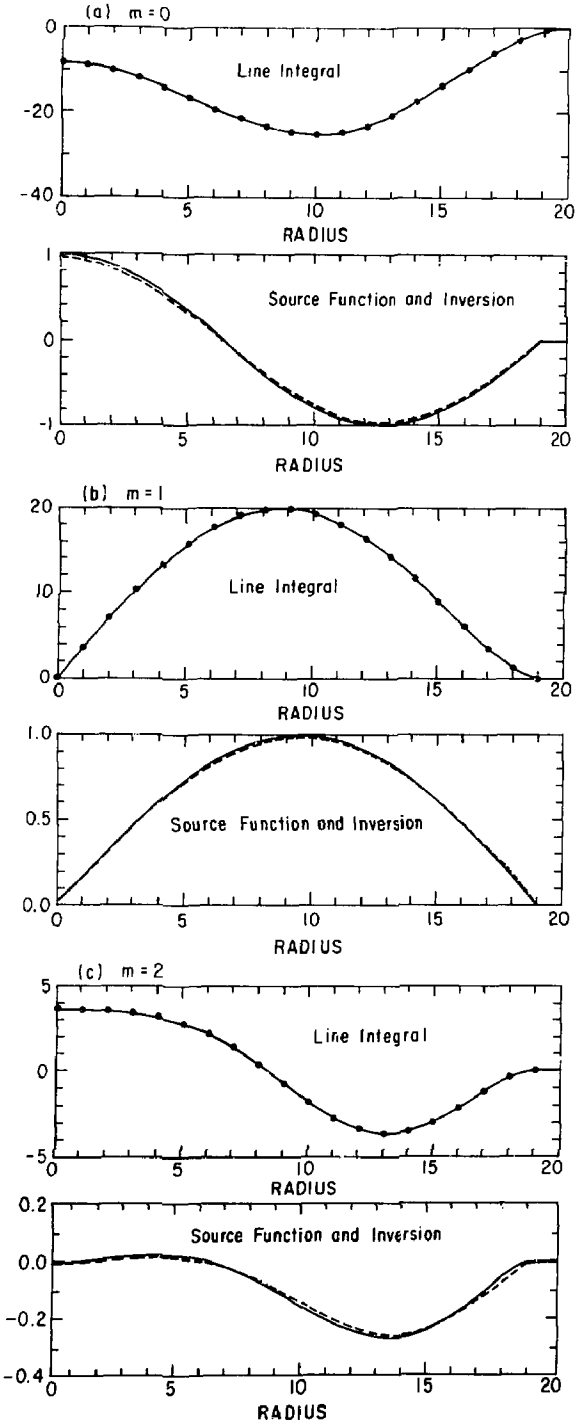
(a) m = 0
Line Integral
RADIUS
Source Function and Inversion
RADIUS
(b) m = 1
Line Integral
RADIUS
Source Function and Inversion
RADIUS
(c) m = 2
Line Integral
RADIUS
Source Function and Inversion
RADIUS

Fig. 3. 783673

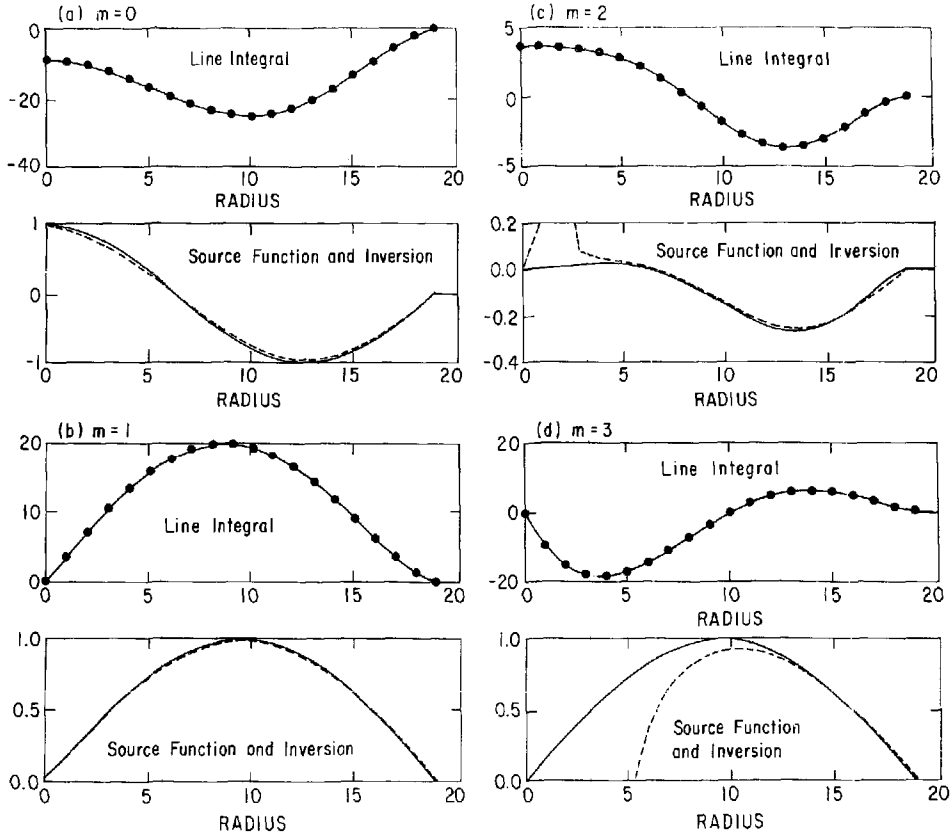
(a) m = 0
Line Integral
RADIUS
Source Function and Inversion
RADIUS
(c) m = 2
Line Integral
RADIUS
Source Function and Inversion
RADIUS
(b) m = 1
Line Integral
Source Function and Inversion
RADIUS
(d) m = 3
Line Integral
RADIUS
Source Function
and Inversion
RADIUS

Fig. 4. 783674

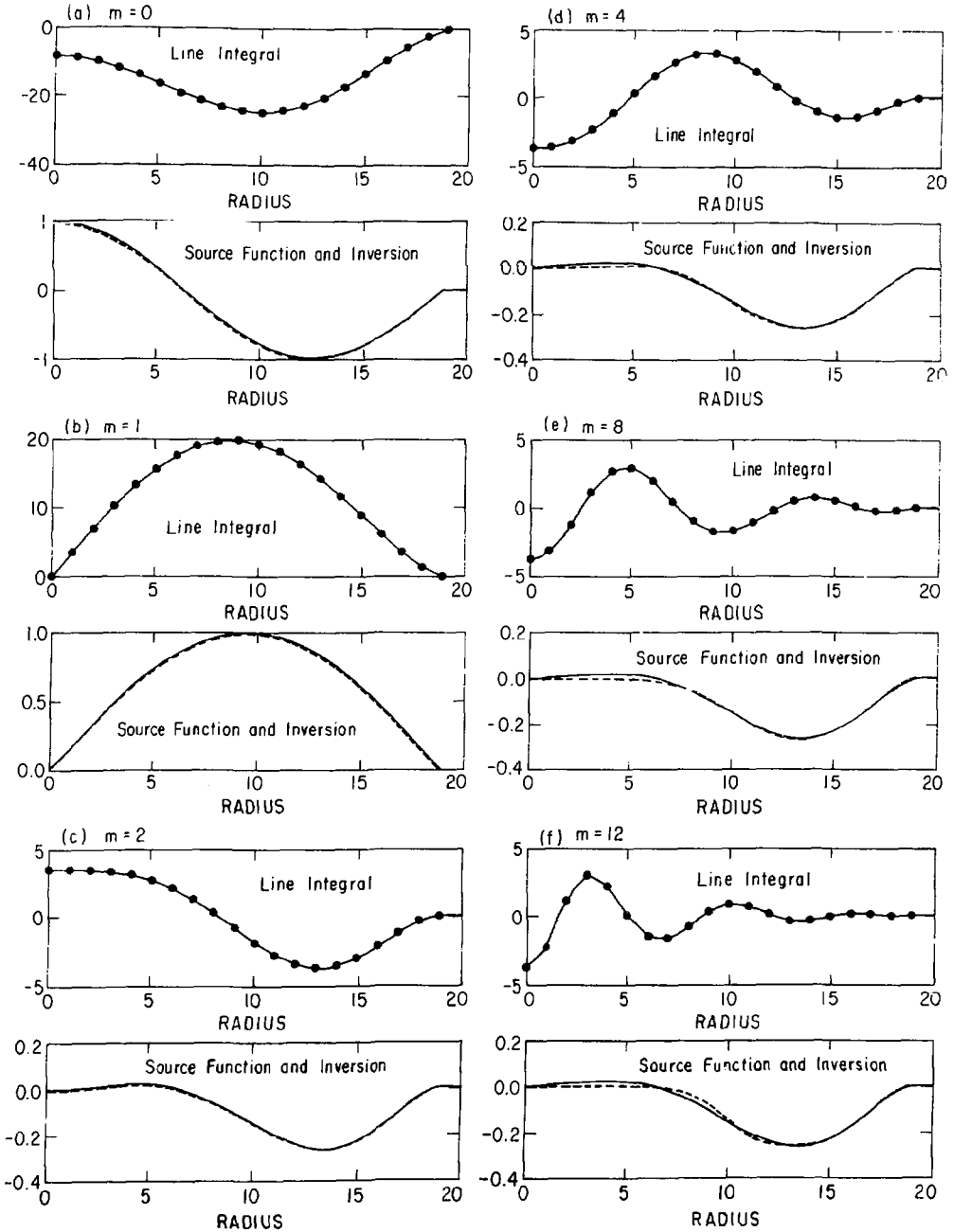
(a) m = 0
Line Integral
RADIUS
Source Function and Inversion
RADIUS
(b) m = 1
Line Integral
RADIUS
Source Function and Inversion
RADIUS
(c) m = 2
Line Integral
RADIUS
Source Function and Inversion
RADIUS
(d) m = 4
Line Integral
RADIUS
Source Function and Inversion
RADIUS
(e) m = 8
Line Integral
RADIUS
Source Function and Inversion
RADIUS
(f) m = 12
Line Integral
RADIUS
Source Function and Inversion
RADIUS

Fig. 5. 783675

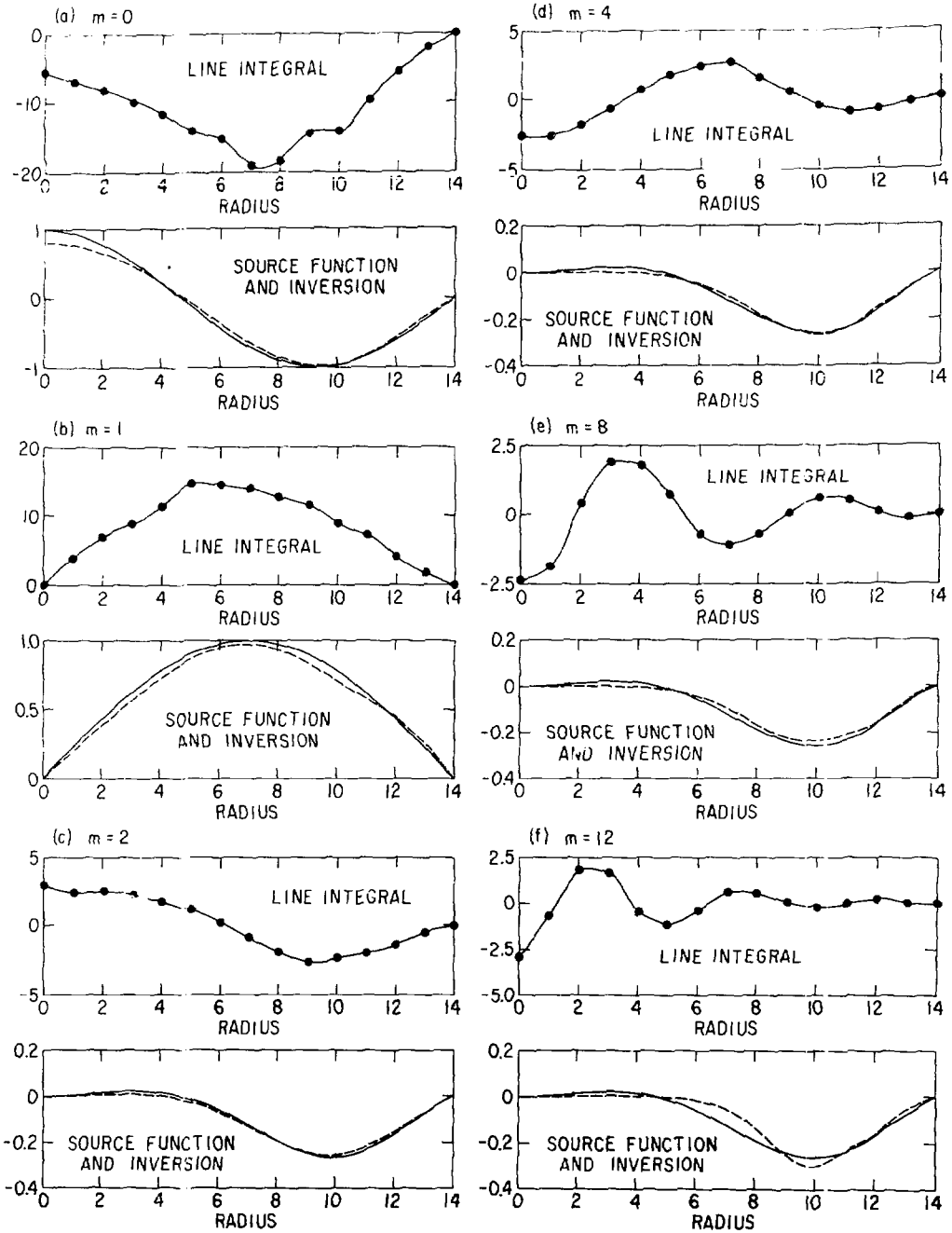
(a) m = 0
LINE INTEGRAL
RADIUS
SOURCE FUNCTION AND INVERSION
RADIUS
(b) m = 1
LINE INTEGRAL
RADIUS
SOURCE FUNCTION AND INVERSION
RADIUS
(c) m = 2
LINE INTEGRAL
RADIUS
SOURCE FUNCTION AND INVERSION
RADIUS
(d) m = 4
LINE INTEGRAL
RADIUS
SOURCE FUNCTION AND INVERSION
RADIUS
(e) m = 8
LINE INTEGRAL
RADIUS
SOURCE FUNCTION AND INVERSION
RADIUS
(f) m = 12
LINE INTEGRAL
RADIUS
SOURCE FUNCTION AND INVERSION
RADIUS

Fig. 6. 783676